Macroscopic Borromean and anti-Borromean states of quantized vortices

Wei-Can Yang [1,*] Makoto Tsubota [1,2] Muneto Nitta,[3,4] and Hua-Bi Zeng[5,†]

[1]*Department of Physics, Osaka Metropolitan University, 3-3-138 Sugimoto, Osaka 558-8585, Japan*

[2]*Nambu Yoichiro Institute of Theoretical and Experimental Physics (NITEP), Osaka Metropolitan University, 3-3-138 Sugimoto, Sumiyoshi-ku, Osaka 558-8585, Japan*

[3]*Research and Education Center for Natural Sciences, Keio University, Hiyoshi 4-1-1, Yokohama, Kanagawa 223-8521, Japan*

[4]*International Institute for Sustainability with Knotted Chiral Meta Matter (SKCM^2), Hiroshima University, 1-3-2 Kagamiyama, Higashi-Hiroshima, Hiroshima 739-8511, Japan*

[5]*Center for Theoretical Physics, Hainan University, Haikou 570228, China*

(Received 8 July 2024; revised 20 October 2024; accepted 5 February 2025; published 13 February 2025)

Borromean states refer to a class of bound states with special topological structures, generally thought to exist only in microscopic systems. In this paper, we investigate vortex bound states in three-component Bose-Einstein condensates using coupled Gross-Pitaevskii equations. Specifically, through the competition between two-body and three-body interactions, we identify the emergence of vortex Borromean states, where only three vortices form a stable bound state while any two-vortex subsystems remain unbound. Our theoretical analysis and numerical simulations provide a comprehensive phase diagram of the vortex Borromean states. Additionally, we uncover an unconventional topological phase—a vortex anti-Borromean state—in which two vortices bind together but separate upon the addition of a third vortex. This study highlights the complex role of three-body interactions in macroscopic systems and offers different insights into the topology and phase transitions of multicomponent vortex systems.

DOI: 10.1103/PhysRevA.111.023319

I. INTRODUCTION

In quantum physics, many-body interactions often lead to unexpected and intriguing behaviors, revealing subtle correlation mechanisms among particles in complex systems. An interesting phenomenon is that bound states with three or more components may be easier to implement than two-body bound states. These special bound states are known as the Borromean state, named after the Borromean rings where three rings are intertwined in a delicate topological manner [see Fig. 1(a)]; if any one ring is removed, the remaining two become unlinked [1].

In few-body physics, this concept is widely accepted and has been validated in phenomena such as halo nuclei in nuclear physics [2–4] and the Efimov effect in ultracold atomic systems [5,6]. The Efimov effect demonstrates that even when two-body interactions are too weak to form a two-body bound state, three particles can still bind together through effective long-range three-body interactions. By utilizing Feshbach resonance tuning, these bound states have been successfully identified in cold atom experiments via three-body loss measurements [7–15]. Therefore, the Borromean binding represents a significant discovery and universal behavior in few-body physics.

In recent years, numerous studies have attempted to explore Borromean binding in many-body physics. One particularly notable discovery is that quantum fluctuations [Lee-Huang-Yang (LHY) corrections] can stabilize three-component droplets forming self-bound states while any binary subsystems cannot, meeting the Borromean criteria [16]. However, to date, a truly macroscopic Borromean bound state has yet to be discovered. When considering macroscopic objects that exhibit quantum effects, the first candidates that come to mind are quantum vortices. These topological defects, which exist widely in superconductors and superfluids, possess stable quantized circulation. Given their quantum nature and macroscopic observability, quantum vortices become ideal candidates for realizing macroscopic Borromean binding.

Recent experimental advances have also pointed to the possibility of tunable many-body interactions in ultracold atom systems. Experiments using Feshbach resonances have demonstrated precise control over both two-body and three-body interactions, allowing researchers to observe Efimov states and related phenomena in multicomponent systems [17,18], especially for three-component ^{6}Li mixtures [19–23]. In addition to tuning the Feschbach resonance, newer methods such as the periodic drive of the Floquet egineering [24,25] and the optical lattices driven by microwave fields [26,27] demonstrated that three-body interactions can be tuned independently of two-body interactions without three-body loss. By leveraging these advances in controlling three-body interactions, it becomes feasible to explore the possibility of a vortex Borromean state in three-component Bose gas.

II. MODEL

In this work, we employed coupled Gross-Pitaevskii equations to study a three-component Bose gas, with a particular

*Contact author: weicanyang@outlook.com
†Contact author: zenghuabi@hainanu.edu.cn

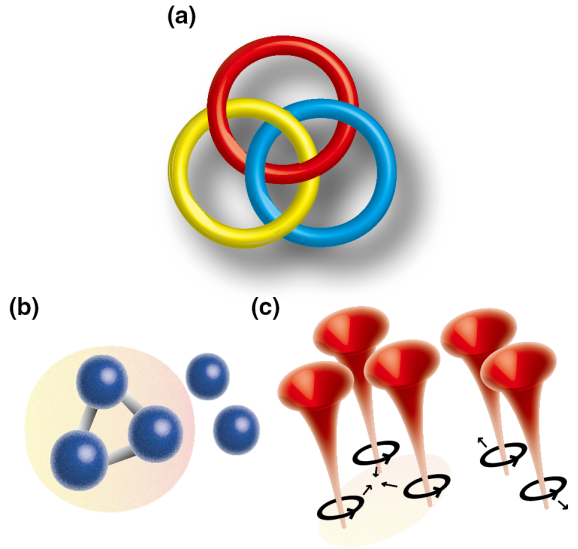

FIG. 1. (a) Borromean ring. (b) Particle Borromean state: Efimov effect. (c) Vortex Borromean state.

focus on the effects of three-body interactions [26]:

$$V_{\text{eff}} = \sum_{i<j} V(\mathbf{r}_i - \mathbf{r}_j) + \sum_{i<j<k} U(\mathbf{r}_i, \mathbf{r}_j, \mathbf{r}_k). \tag{1}$$

Our study revealed that vortices can form special Borromean bound states, in which three vortices can form a bound state, but removing any vortex causes the remaining vortex pairs to separate [Fig. 1(c)].

To illustrate the three-body interactions in a three-component Bose gas, we consider the system's energy expressed in terms of the macroscopic wave functions. The three-body interaction term is represented in an effective form [26,28,29], benefiting from recent advances in experimental techniques that allow for the independent manipulation of three-body interactions. This approach captures the main contributions of such interactions to the system's dynamics [30,31]:

$$\begin{aligned} E(\Psi) &= \int d^3x[K(\Psi) + V(\Psi)], \\ K(\Psi) &= \sum_{i=1,2,3} \left(-\frac{\hbar^2}{2m_i} \Psi_i^* \nabla^2 \Psi_i \right), \\ V(\Psi) &= \sum_{i=1,2,3} \frac{g_i}{2} |\Psi_i|^4 + \sum_{i,j=1,2,3}^{i\neq j} \frac{g_{ij}}{2} |\Psi_i|^2 |\Psi_j|^2 \\ &\quad + g_{123} |\Psi_1|^2 |\Psi_2|^2 |\Psi_3|^2. \end{aligned} \tag{2}$$

We assume that the three components are distinct hyperfine states of the same atom, such as the spin-1 ^{87}Rb BEC system, resulting in identical atomic masses m and intracomponent interaction strengths g. Here, g_{ij} and g_{123} represent the two-body and three-body interaction coefficients, respectively. Our model focuses exclusively on intercomponent three-body interactions, while neglecting intracomponent effects. This is because intracomponent interactions primarily influence the properties of individual vortices, such as their size and core structure, rather than the interactions between vortices in different components. Consequently, they do not exert a qualitative influence on the macroscopic phenomena under investigation.

By applying the variational principle to minimizing free energy $i\hbar\partial_t \Psi_i = \delta F/\delta \Psi_i^* = \delta(E - \mu N)/\delta \Psi_i^*$, where μ is the chemical potential and N is the particle number $\int |\psi|^2$, we can derive the equations of motion from the energy functional, resulting in the coupled three-component Gross-Pitaevskii (GP) equations that include three-body interactions,

$$(i\hbar\partial_t + \mu)\Psi_i = \left(-\frac{\hbar^2\nabla^2}{2m} + g|\Psi_i|^2 + \eta(|\Psi_j|^2 + |\Psi_k|^2) + \epsilon|\Psi_j|^2|\Psi_k|^2 \right) \Psi_i(i, j, k) \text{ is a cyclic permutation of } (1, 2, 3). \tag{3}$$

Here, to ensure the identical nature of the interactions among the three vortices, we choose $g_{ij} = \eta$ and $g_{123} = \epsilon$.

Further, by consider a time dependence $\partial_t \Psi_i = 0$, we can obtain the stationary equation with the ground state wave function

$$\mu\Psi_i = \left(-\frac{\hbar^2\nabla^2}{2m} + g|\Psi_i|^2 + \eta(|\Psi_j|^2 + |\Psi_k|^2) + \epsilon|\Psi_j|^2|\Psi_k|^2 \right) \Psi_i, \quad |\Psi_i|^2 \equiv v^2 = \frac{\sqrt{4\epsilon\mu + (2\eta + g)^2} - (2\eta + g)}{2\epsilon}. \tag{4}$$

The topology of its ground state is characterized $\pi_1[U(1)^3] = \mathbb{Z} \oplus \mathbb{Z} \oplus \mathbb{Z}$. It allows three kinds of winding numbers [refer to (1,0,0), (0,1,0), (0,0,1)]. When moving around the (1,0,0)[(0,1,0),(0,0,1)] vortex, the phase of $\Psi_1(\Psi_2, \Psi_3)$ rotates by 2π, while the phases of the other components remain unchanged. Similarly, we can obtain representations of multivortex structures such as (1,1,0) and (1,1,1) [32,33].

III. VORTEX PROFILE AND INTERACTION

As a starting point, we can express the axisymmetric structure of a single vortex with quantum numbers (1,0,0) by writing its different components in the following form,

$$\begin{aligned} \Psi_1^{(1,0,0)} &= ve^{i\theta} f_{(1,0,0)}(r), \\ \Psi_2^{(1,0,0)} &= vh_{(1,0,0)}(r), \\ \Psi_3^{(1,0,0)} &= vl_{(1,0,0)}(r), \end{aligned} \tag{5}$$

where r and θ are the polar coordinates. The phase term θ is present only in the first component, where the vortex is located. The profile functions $f_{(1,0,0)}$, $h_{(1,0,0)}$, and $l_{(1,0,0)}$ can be obtained by substituting vortex configuration function in Eq. (5) into stationary Eq. (4) with the boundary condition $(f_{(1,0,0)}, h_{(1,0,0)}, l_{(1,0,0)}) \to (1, 1, 1)$ as $r \to \infty$ and $f_{(1,0,0)} \to 0$ as $r \to 0$.

We adopt a common yet practical vortex structure as a trial solution and improved the profile function trial solutions for other components based on this, satisfying the boundary conditions with the fullest degrees of freedom [34]:

$$\begin{aligned} f_{(1,0,0)}(r) &= \frac{r}{\sqrt{a+r^2}}, \\ h_{(1,0,0)}(r) &= 1+c-\frac{cr}{\sqrt{b+r^2}}, \\ l_{(1,0,0)}(r) &= 1+c-\frac{cr}{\sqrt{b+r^2}}. \end{aligned} \tag{6}$$

By substituting these trial solutions into the GP equation, we can obtain the correct coefficient relations for the vortex profile functions,

$$\begin{aligned} a &= \frac{p^+}{(p^+-2p^-)(p^++p^-)}\frac{\hbar^2}{2v^2m}, \\ b\times c &= \frac{p^-}{(p^+-2p^-)(p^++p^-)}\frac{\hbar^2}{2v^2m}, \end{aligned} \tag{7}$$

where $p^+ = g+\eta+v^2\epsilon$ and $p^- = \eta+v^2\epsilon$. From this structure, we can obviously find that the instability condition shifts from the two-component phase separation $g<\eta$ [35] to the inclusion of three-body interactions in $g<\eta+v^2\epsilon$. If $g>\eta+v^2\epsilon$, a is always positive while the sign of $b\times c$ depends on the parameter $p^- = v^2\epsilon+\eta$. From the profile function $h_{(1,0,0)}$ and $l_{(1,0,0)}$, c should be a small value and b should be a positive value. Since $v^2=\rho_s$ is the background density, we know then that the profile function of the unwinding component at the vortex center is concave for $\rho_s\epsilon+\eta<0$ and convex for $\rho_s\epsilon+\eta>0$. Profile functions of vortices in the other cases (0,1,0) and (0,0,1) can be obtained in the same way.

With these structured functions, we can proceed to calculate the interactions between two and three vortices. The initial vortex distribution can be set up using a polar coordinate system.

For example, consider two well-separated vortices (1,0,0) and (0,1,0) in different components. Let us place the (1,0,0) and (0,1,0) vortices at $(x,y)=(R,0)$ and $(x,y)=(-R,0)$, respectively. We use the polar coordinates (r,θ) with the origin $(x,y)=(0,0)$ and express the relative coordinates from (1,0,0) and (0,1,0) vortex center as $[r_{(1,0,0)},\theta_{(1,0,0)}]$ and $[r_{(0,1,0)},\theta_{(0,1,0)}]$. Then we have

$$\begin{aligned} r_i^2 &= (r\cos\theta\mp R)^2+r^2\sin^2\theta = (x\mp R)^2+y^2, \\ \tan\theta_i &= \frac{r\sin\theta}{r\cos\theta\mp R} = \frac{y}{x\mp R}, \end{aligned} \tag{8}$$

with $i=1$ or $(1,0,0)$, 2 or $(0,1,0)$, the minus sign for $i=1$ or $(1,0,0)$, and the plus sign for $i=2$ or $(0,1,0)$. Then the vortex configurations can be expressed as

$$\psi_1^{(1,0,0)} = ve^{i\theta_{(1,0,0)}}f_{(1,0,0)}[r_{(1,0,0)}] = ve^{i\theta_1}\left(\frac{r_1}{\sqrt{a+r_1^2}}\right),$$

$$\psi_2^{(1,0,0)} = vh_{(1,0,0)}[r_{(1,0,0)}] = v\left(1+c-\frac{cr_1}{\sqrt{b+r_1^2}}\right),$$

$$\psi_3^{(1,0,0)} = vl_{(1,0,0)}[r_{(1,0,0)}] = v\left(1+c-\frac{cr_1}{\sqrt{b+r_1^2}}\right),$$

$$\psi_1^{(0,1,0)} = vh_{(0,1,0)}[r_{(0,1,0)}] = v\left(1+c-\frac{cr_2}{\sqrt{b+r_2^2}}\right),$$

$$\psi_2^{(0,1,0)} = ve^{i\theta_{(0,1,0)}}f_{(0,1,0)}[r_{(0,1,0)}] = ve^{i\theta_2}\left(\frac{r_2}{\sqrt{a+r_2^2}}\right),$$

$$\psi_3^{(0,1,0)} = vl_{(0,1,0)}[r_{(0,1,0)}] = v\left(1+c-\frac{cr_2}{\sqrt{b+r_2^2}}\right).$$

Similarly, in the three-vortex case, we can consider the third vortex (0,0,1) that be placed at $(x,y)=(0,\sqrt{3})$. Thus, the three vortices form a C_3 rotationally symmetric structure,

$$\begin{aligned} r_{(0,0,1)}^2 &= r^2\sin^2\theta+(r\cos\theta-\sqrt{3}R)^2, \\ \tan\theta_{(0,0,1)} &= \frac{r\cos\theta-\sqrt{3}R}{r\sin\theta}, \end{aligned} \tag{9}$$

and we can write the profile function caused by the three vortices in each component. Using these structures allows for precise calculations of vortex interactions.

With these vortex structures and profile functions, we can calculate the actual vortex interactions. In the case of two vortices, the interaction potential can be obtained by subtracting the individual energies from the total energy as

$$U_{(1,1,0)} = \int d^2x(\delta K_{(1,1,0)}+\delta V_{(1,1,0)}), \tag{10}$$

where two contributions come from the kinetics energy $\delta K_{(1,1,0)} = K(\Psi_i^{(1,1,0)})-K(\Psi_i^{(1,0,0)})-K(\Psi_i^{(0,1,0)})$ and the interaction potential energy $\delta V_{(1,1,0)} = V(\Psi_i^{(1,1,0)})-V(\Psi_i^{(1,0,0)})-V(\Psi_i^{(0,1,0)})$, where $\Psi_i^{(1,1,0)}$ come from the standard Abrikosov ansatz $\Psi_1^{(1,1,0)} = v^{-1}\Psi_i^{(1,0,0)}\Psi_i^{(0,1,0)}$ [36]. Then, by using the derivation of the interaction potential with respect to the distance, one can then calculate the interaction force

$$F_{(1,1,0)} = -\frac{\partial U_{(1,1,0)}}{2\partial R}. \tag{11}$$

For the three-vortex case, we repeat the above steps, but consider replacing one of the vortices with a vortex pair,

$$\begin{aligned} U_{(1,1,1)} &= \int d^2x(\delta K_{(1,1,1)}+\delta V_{(1,1,1)}), \\ F_{(1,1,1)} &= -\frac{\partial U_{(1,1,1)}}{3\partial R}, \end{aligned} \tag{12}$$

with contributions from the kinetic energy $\delta K_{(1,1,1)} = K(\Psi_i^{(1,1,1)})-K(\Psi_i^{(1,1,0)})-K(\Psi_i^{(0,0,1)})$ and interaction

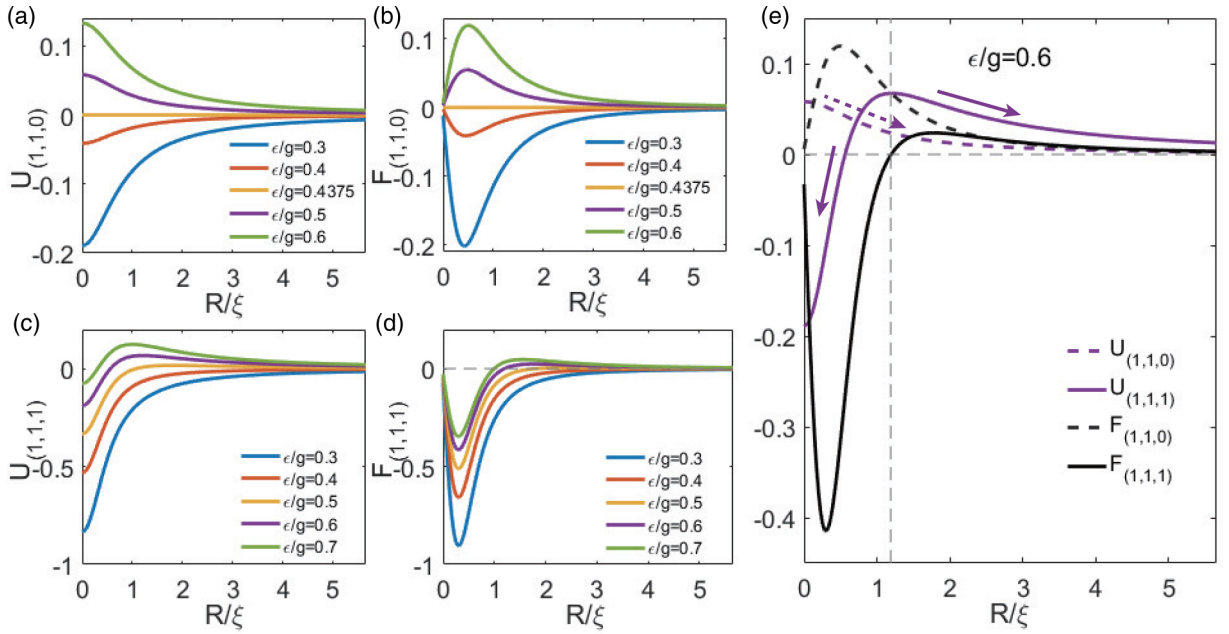

FIG. 2. Vortex interaction potential and force as the function of distance. (a), (b) Interaction between two vortices. From top to bottom, the three-body interaction decreases; at $p^- = 0$ ($\epsilon = 0.4375g$), there is no interaction between two vortices. (c), (d) For the same parameters, the three-vortex interaction becomes nonmonotonic when $p^- > 0$: The vortices attract each other below a critical distance and repel above it. (e) Interaction diagram showing vortex Borromean binding at $\epsilon = 0.6g$. Below the critical distance, three vortices attract while two vortices repel.

potential energy $\delta V_{(1,1,1)} = V(\Psi_i^{(1,1,1)}) - V(\Psi_i^{(1,1,0)}) - V(\Psi_i^{(0,0,1)})$, where $\Psi_i^{(1,1,1)} = v^{-2}\psi_i^{(1,0,0)}\Psi_i^{(0,1,0)}\Psi_i^{(0,0,1)}$.

IV. VORTEX BORROMEAN STATE

We start with a simple assumption: For the sake of convenience, we assume the small quantity c to be 0. This implies that the vortex does not induce fluctuations in the other components, with $h(r) = l(r) = 1$. We will later demonstrate that this assumption is entirely reasonable when the coupling strength is not sufficiently large. This simplification allows us to more easily calculate the interaction between two vortices,

$$U_{(1,1,0)} = a^2\pi v^4(\eta + v^2\epsilon)\frac{\operatorname{arctanh}(R/\sqrt{R^2+a})}{R\sqrt{R^2+a}},$$
$$F_{(1,1,0)} = -1/2a^2\pi v^4(\eta + v^2\epsilon) \times \frac{R\sqrt{a+R^2} - (a+2R^2)\operatorname{arctanh}\left(\frac{R}{\sqrt{a+R^2}}\right)}{R^2(a+R^2)^{3/2}}. \quad (13)$$

We observe that in the case of two vortices, the vortex interaction direction depends only on $p^- = \eta + v^2\epsilon$. Without loss of generality, we use the parameters $\hbar = m = 1$, $g = 7$, $\mu = 4$, and fix $\eta = -0.5g$ with the scales of length and time by the characteristic value $\xi = \sqrt{\hbar^2/2m\mu}$ and $\tau = \hbar/\mu$ [37]. As shown in Figs. 2(a) and 2(b), as ϵ gradually increases, the interaction force remains negative when $p^- < 0$ ($\epsilon/g < 0.4375$), representing an attractive force between the two vortices. When $p^- > 0$, the force becomes positive, and the two vortices repel each other. This indicates that the interaction direction between the two vortices does not change with distance and is monotonic.

However, for the three-vortex case, we find that the potential energy is

$$U_{(1,1,1)} = \int d^2x v^4[\eta(1-k_3)(1-k_1) + \eta(1-k_3)(1-k_2) + v^2\epsilon(1-k_1k_2)(1-k_3)], \quad (14)$$

where $k_{(1,2,3)} = \frac{r^2_{(1,2,3)}}{a+r^2_{(1,2,3)}}$ and r_i refers to the coordinate position relative to vortex i. This integral is difficult to solve analytically, but from its form, we can see that it is no longer a monotonic function dependent only on p^-. We can use high-precision discrete methods for numerical integration to simultaneously obtain the interaction force $F_{(1,1,1)} = -\partial U_{(1,1,1)}/3\partial R$.

Figures 2(c) and 2(d) show the interaction potential energy and force for three vortices, using the same parameters as in the two-vortex case shown in Figs. 2(a) and 2(b). It can be observed that in the case of three vortices, when $p^- > 0$, there is a critical distance R_c. Below this critical distance, the vortices attract each other; above this critical distance, the vortices repel each other. In Fig. 2(e), we selected one of the parameters $\epsilon = 0.6g$ to compare the interactions between two vortices and three vortices directly. On the left side of the critical distance indicated by the dashed line, the two vortices repel each other while the three vortices attract each other. This indicates the emergence of a new vortex state, whose topological structure remarkably aligns with the Borromean rings. We refer to this phenomenon as the vortex Borromean binding.

We validated this theoretical result through numerical simulations of the dynamical evolution of the equations of motion in Eq. (3). The actual simulation results of vortex dynamics are provided in Fig. 3 and in a movie in the Supplemental

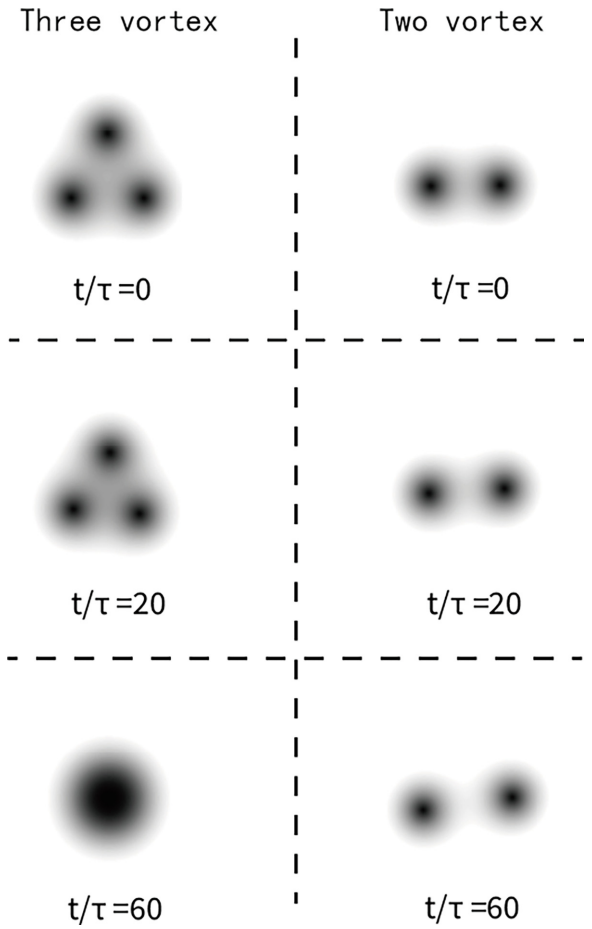

FIG. 3. The dynamic evolution of vortex Borromean states with $\epsilon = 0.6g$ and $R/\xi = 1$. Finally, the three vortices approach each other to form a giant vortex, while the two vortices completely separate.

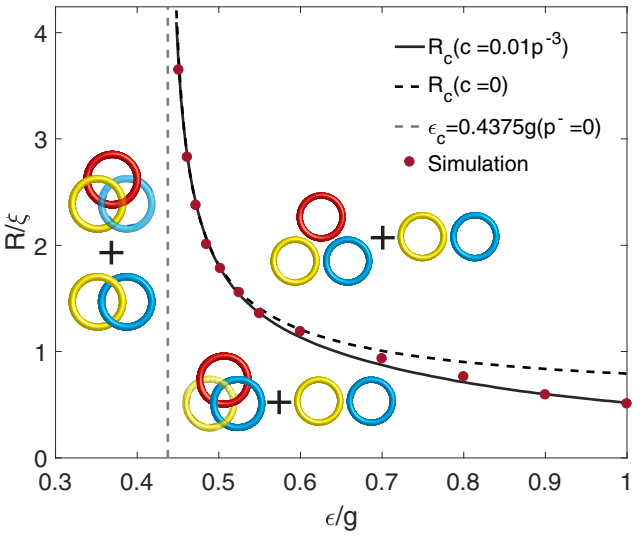

FIG. 4. Phase diagram of vortex Borromean states with fixed $\eta/g = -0.5$. Three-ring diagrams illustrate how three vortices interact; adjacent two-ring diagrams show whether the remaining two vortices are bound when the red ring is removed. The left structure represents the fully bound state, the bottom shows the Borromean states, and the right depicts the completely unbound state. The dashed curve represents ideal vortex calculations with $c = 0$, the solid curve represents calculations with $c = 0.01(p^-)^3$, and the red dots indicate numerical simulation results.

Material [38]. It can be observed that, starting from the same initial distance, three vortices gradually attract each other, forming a giant vortex, while two vortices gradually move apart until they no longer interact.

By repeatedly performing numerical simulations with varying initial vortex distances, we can obtain the phase diagram of the vortex Borromean states, showing the variation of the critical distance with three-body interactions, as shown in Fig. 4. On the left side of the critical p_c^- ($\epsilon_c = 0.4375g$), there is the fully bound state phase where the three vortices (rings) are completely intertwined, and even if one vortex (ring) is removed, the remaining two are still entangled. On the right side of the critical p_c^-, there are two phases: When the distance is greater than the critical value, it is the completely unbound state phase; when the distance is less than the critical value, it is the vortex Borromean states, where the binding of each pair of vortices (rings) is mediated by the third vortex (ring). If one vortex (ring) is removed, the remaining two are unbound.

From the critical distance we can find that when the coupling constant ϵ is small, the theoretical results under the ($c = 0$) approximation match well to the actual simulation values. However, when ϵ is large, this approximation is no longer valid, because the vortex profile deformation can no longer be ignored, so we need to consider a finite c. By examining the vortex profile functions, a reasonable analysis can be made here. Assuming that c is a small value and proportional to $(p^-)^d$, then c and b should be modified as follows,

$$c = t(p^-)^d,$$
$$b = \frac{1}{t}\frac{1}{(p^-)^{d-1}(p^+ - 2p^-)(p^+ + p^-)}\frac{\hbar^2}{2v^2m}, \qquad (15)$$

so that when using the parameters $t = 0.01$ and $d = 3$, we observe that the theoretical results are in complete agreement with the numerical simulation outcomes. As a result, we have obtained a more accurate theoretical phase diagram in Fig. 4, which further validates the accuracy of our trial solutions.

Through a comprehensive scan of η and ϵ, we have further mapped out the complete phase diagram of the vortex Borromean states, as illustrated in Fig. 5. We systematically scanned all regions with a $\delta\eta = \delta\epsilon = 0.01$ interval, identifying the nonzero R_c regions where the vortex Borromean states occur. This analysis clearly shows that the vortex Borromean states emerge in all regions where $p^- = \eta + v^2\epsilon > 0$, indicating that the phenomenon is highly controllable. For experimental observations, this suggests that identifying the interaction range where $p^- > 0$ could enable the detection of the vortex Borromean states.

V. VORTEX ANTI-BORROMEAN STATE

All the results discussed above were obtained under the condition of negative two-body interaction η. In Fig. 6, we explored the region with positive two-body coupling and discovered another vortex topological phenomenon: vortex anti-Borromean states. This discovery is remarkably

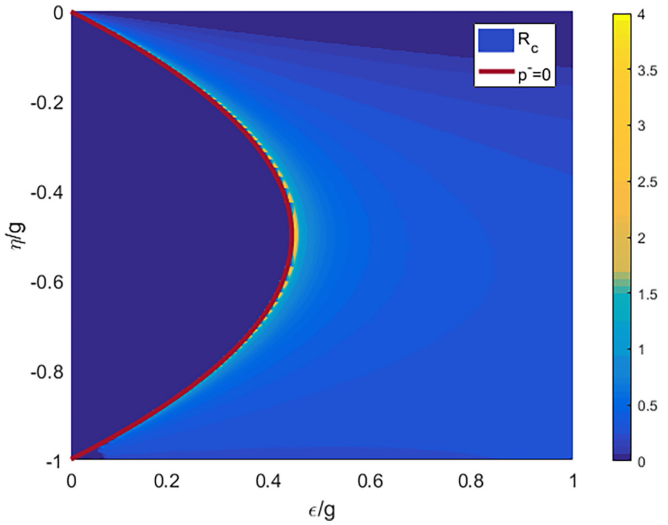

FIG. 5. The complete phase diagram of the vortex Borromean states. The color bar indicates critical distance; the red line shows $p^{-} = 0$. Zero critical distance (left region) means no vortex Borromean states.

counterintuitive—unlike the conventional Borromean ring topology, where three bodies are interlinked and removing one causes the entire structure to collapse, the anti-Borromean states demonstrate the opposite behavior. In this effect, two vortices form a stable bound state, but the introduction of a third vortex causes the system to unbind, breaking the established topological linkage. This interaction leads to a topological structure that is difficult to intuitively visualize, as it breaks from the typical understanding of how such systems should behave, which typically rely on the concept of mutual dependence among all components for stability. Such results suggest that the range of possible topological configurations in quantum many-body systems is more diverse than traditionally thought, beyond those previously imagined in particle systems, potentially leading to the discovery of new quantum phases and transitions.

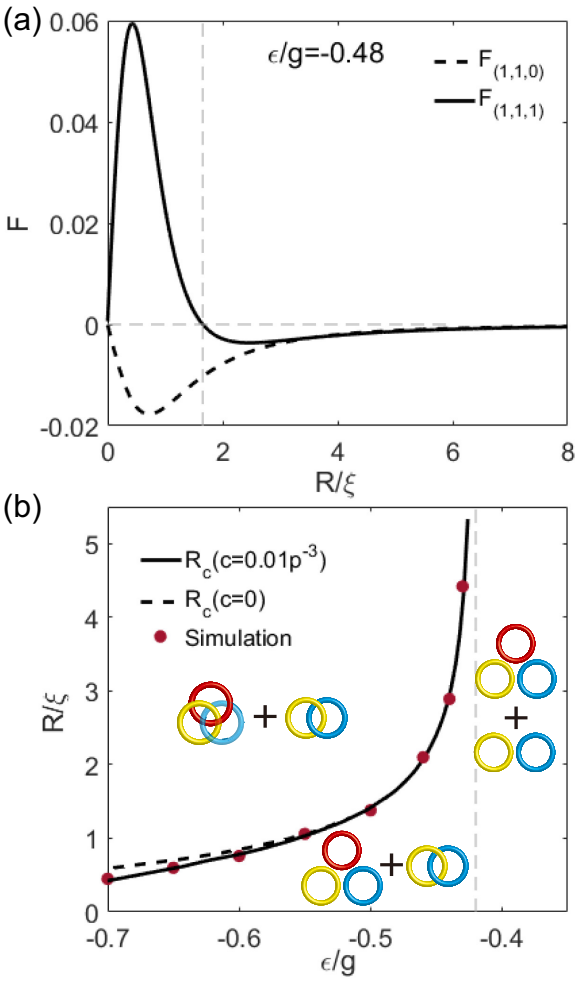

FIG. 6. (a) The interaction force displaying the vortex anti-Borromean states by fixed $\eta = 0.3g$ and $\epsilon = -0.48g$. On the left side of the critical distance represented by the dashed line, the three vortices have repulsive interactions, while the two vortices attract each other (for a specific simulation, see the movie in the Supplemental Material [38]). (b) Phase diagram of vortex anti-Borromean states with fixed $\eta = 0.3g$.

VI. DISCUSSION

Our results provide a convincing (theoretical and numerical) case of extending the Borromean bound states to a macroscopic vortex system. The significance of the vortex Borromean states lies in its observational advantages: The vortex Borromean states provides a unique opportunity to visually or directly observe the three-body interaction and the formation of the Borromean ring structure. In addition, the vortex anti-Borromean states go beyond the theoretical scope of few-body physics, which represents an unexpected reversal of Borromean topology, reflecting the unique influence of three-body interactions in macroscopic systems.

For experimental realization, the most promising candidate is the spin-1 BEC system, such as that formed with ^{87}Rb atoms, where the three hyperfine states $m_F = \{-1, 0, 1\}$ act as the three components [39]. By utilizing magnetic Feshbach resonances [21,23], the relative strengths of two-body and three-body interactions could be precisely controlled. To create and observe such states, one could first establish the presence of vortices in each component individually using phase imprinting techniques [40], followed by tuning the intercomponent interactions to induce the collective binding of the three vortices. By tracking the motion of the vortices [41,42], one could visually observe the Borromean state in a macroscopic vortex system. In addition to spin-1 BECs, similar theoretical and experimental explorations of the vortex Borromean state can be extended to other vortex systems, such as Fermi superfluids or polar molecule systems, where similar multibody interaction dynamics are anticipated to emerge.

ACKNOWLEDGMENTS

We would like to thank X. Wang, K. Y. Lu, and Q. Y. Zhang for discussions. H.-B.Z. acknowledges the support by the National Natural Science Foundation of China (under Grant

No. 12275233). M.T. acknowledges the support from JSPS KAKENHI Grants No. JP23K03305 and No. JP22H05139. The work of M.N. is supported in part by JSPS KAKENHI (No. JP22H01221) and the WPI program "Sustainability with Knotted Chiral Meta Matter ($SKCM^2$)" at Hiroshima University.

[1] P. Cromwell, E. Beltrami, and M. Rampichini, The mathematical tourist, Math. Intell. **20**, 53 (1998).

[2] D. V. Fedorov, A. S. Jensen, and K. Riisager, Three-body halos: Gross properties, Phys. Rev. C **49**, 201 (1994).

[3] M. Zhukov, B. Danilin, D. Fedorov, J. Bang, I. Thompson, and J. Vaagen, Bound state properties of Borromean halo nuclei: ^{6}He and ^{11}Li, Phys. Rep. **231**, 151 (1993).

[4] K. Tanaka, T. Yamaguchi, T. Suzuki, T. Ohtsubo, M. Fukuda, D. Nishimura, M. Takechi, K. Ogata, A. Ozawa, T. Izumikawa, T. Aiba, N. Aoi, H. Baba, Y. Hashizume, K. Inafuku, N. Iwasa, K. Kobayashi, M. Komuro, Y. Kondo, T. Kubo *et al.*, Observation of a large reaction cross section in the drip-line nucleus ^{22}C, Phys. Rev. Lett. **104**, 062701 (2010).

[5] V. Efimov, Energy levels arising from resonant two-body forces in a three-body system, Phys. Lett. B **33**, 563 (1970).

[6] V. N. Efimov, Weakly bound states of three resonantly interacting particles, Yad. Fiz. **12**, 1080 (1970) [Sov. J. Nucl. Phys. **12**, 589 (1971)].

[7] T. Kraemer, M. Mark, P. Waldburger, J. G. Danzl, C. Chin, B. Engeser, A. D. Lange, K. Pilch, A. Jaakkola, H.-C. Nägerl, and R. Grimm, Evidence for Efimov quantum states in an ultracold gas of caesium atoms, Nature (London) **440**, 315 (2006).

[8] S. Knoop, F. Ferlaino, M. Mark, M. Berninger, H. Schöbel, H.-C. Nägerl, and R. Grimm, Observation of an Efimov-like trimer resonance in ultracold atom–dimer scattering, Nat. Phys. **5**, 227 (2009).

[9] M. Zaccanti, B. Deissler, C. D'Errico, M. Fattori, M. Jona-Lasinio, S. Müller, G. Roati, M. Inguscio, and G. Modugno, Observation of an Efimov spectrum in an atomic system, Nat. Phys. **5**, 586 (2009).

[10] S. E. Pollack, D. Dries, and R. G. Hulet, Universality in three- and four-body bound states of ultracold atoms, Science **326**, 1683 (2009).

[11] B. Huang, L. A. Sidorenkov, R. Grimm, and J. M. Hutson, Observation of the second triatomic resonance in Efimov's scenario, Phys. Rev. Lett. **112**, 190401 (2014).

[12] S.-K. Tung, K. Jiménez-García, J. Johansen, C. V. Parker, and C. Chin, Geometric scaling of Efimov states in a ^{6}Li - ^{133}Cs mixture, Phys. Rev. Lett. **113**, 240402 (2014).

[13] J. Johansen, B. J. DeSalvo, K. Patel, and C. Chin, Testing universality of Efimov physics across broad and narrow Feshbach resonances, Nat. Phys. **13**, 731 (2017).

[14] R. Pires, J. Ulmanis, S. Häfner, M. Repp, A. Arias, E. D. Kuhnle, and M. Weidemüller, Observation of Efimov resonances in a mixture with extreme mass imbalance, Phys. Rev. Lett. **112**, 250404 (2014).

[15] M. Kunitski, S. Zeller, J. Voigtsberger, A. Kalinin, L. P. H. Schmidt, M. Schöffler, A. Czasch, W. Schöllkopf, R. E. Grisenti, T. Jahnke, D. Blume, and R. Dörner, Observation of the Efimov state of the helium trimer, Science **348**, 551 (2015).

[16] Y. Ma, C. Peng, and X. Cui, Borromean droplet in three-component ultracold Bose gases, Phys. Rev. Lett. **127**, 043002 (2021).

[17] L. J. Wacker, N. B. Jørgensen, D. Birkmose, N. Winter, M. Mikkelsen, J. Sherson, N. Zinner, and J. J. Arlt, Universal three-body physics in ultracold KrB mixtures, Phys. Rev. Lett. **117**, 163201 (2016).

[18] U. Eismann, L. Khaykovich, S. Laurent, I. Ferrier-Barbut, B. S. Rem, A. T. Grier, M. Delehaye, F. Chevy, C. Salomon, L.-C. Ha, and C. Chin, Universal loss dynamics in a unitary Bose gas, Phys. Rev. X **6**, 021025 (2016).

[19] T. B. Ottenstein, T. Lompe, M. Kohnen, A. N. Wenz, and S. Jochim, Collisional stability of a three-component degenerate Fermi gas, Phys. Rev. Lett. **101**, 203202 (2008).

[20] Y. Nishida, New type of crossover physics in three-component Fermi gases, Phys. Rev. Lett. **109**, 240401 (2012).

[21] S. Nakajima, M. Horikoshi, T. Mukaiyama, P. Naidon, and M. Ueda, Nonuniversal Efimov atom-dimer resonances in a three-component mixture of ^{6}Li, Phys. Rev. Lett. **105**, 023201 (2010).

[22] S. Nakajima, M. Horikoshi, T. Mukaiyama, P. Naidon, and M. Ueda, Measurement of an Efimov trimer binding energy in a three-component mixture of ^{6}Li, Phys. Rev. Lett. **106**, 143201 (2011).

[23] J. R. Williams, E. L. Hazlett, J. H. Huckans, R. W. Stites, Y. Zhang, and K. M. O'Hara, Evidence for an excited-state Efimov trimer in a three-component Fermi gas, Phys. Rev. Lett. **103**, 130404 (2009).

[24] F. Petiziol, M. Sameti, S. Carretta, S. Wimberger, and F. Mintert, Quantum simulation of three-body interactions in weakly driven quantum systems, Phys. Rev. Lett. **126**, 250504 (2021).

[25] A. Hammond, L. Lavoine, and T. Bourdel, Tunable three-body interactions in driven two-component Bose-Einstein condensates, Phys. Rev. Lett. **128**, 083401 (2022).

[26] H. P. Büchler, A. Micheli, and P. Zoller, Three-body interactions with cold polar molecules, Nat. Phys. **3**, 726 (2007).

[27] L. Mazza, M. Rizzi, M. Lewenstein, and J. I. Cirac, Emerging bosons with three-body interactions from spin-1 atoms in optical lattices, Phys. Rev. A **82**, 043629 (2010).

[28] R. D. Murphy and J. A. Barker, Three-body interactions in liquid and solid helium, Phys. Rev. A **3**, 1037 (1971).

[29] P. R. Johnson, E. Tiesinga, J. V. Porto, and C. J. Williams, Effective three-body interactions of neutral bosons in optical lattices, New J. Phys. **11**, 093022 (2009).

[30] P. F. Bedaque and J. P. D'Incao, Superfluid phases of the three-species fermion gas, Ann. Phys. (NY) **324**, 1763 (2009).

[31] D. S. Petrov, Three-body interacting bosons in free space, Phys. Rev. Lett. **112**, 103201 (2014).

[32] M. Eto and M. Nitta, Vortex trimer in three-component Bose-Einstein condensates, Phys. Rev. A **85**, 053645 (2012).

[33] M. Eto and M. Nitta, Vortex graphs as N-omers and $\mathbb{C}P^{N-1}$ skyrmions in N-component Bose-Einstein condensates, Europhys. Lett. **103**, 60006 (2013).

[34] C. J. Pethick and H. Smith, *Bose–Einstein Condensation in Dilute Gases* (Cambridge University Press, Cambridge, UK, 2008).

[35] K. Kasamatsu, M. Tsubota, and M. Ueda, Vortex phase diagram in rotating two-component Bose-Einstein condensates, Phys. Rev. Lett. **91**, 150406 (2003).

[36] M. Eto, K. Kasamatsu, M. Nitta, H. Takeuchi, and M. Tsubota, Interaction of half-quantized vortices in two-component Bose-Einstein condensates, Phys. Rev. A **83**, 063603 (2011).

[37] K. Kasamatsu, M. Eto, and M. Nitta, Short-range intervortex interaction and interacting dynamics of half-quantized vortices in two-component Bose-Einstein condensates, Phys. Rev. A **93**, 013615 (2016).

[38] See Supplemental Material at http://link.aps.org/supplemental/10.1103/PhysRevA.111.023319 for the movies associated with Figs. 3 and 6, which illustrate the three-vortex and two-vortex evolutions in vortex Borromean states and vortex anti-Borromean states.

[39] P. M. A. Mestrom, J.-L. Li, V. E. Colussi, T. Secker, and S. J. J. M. F. Kokkelmans, Three-body spin mixing in spin-1 Bose-Einstein condensates, Phys. Rev. A **104**, 023321 (2021).

[40] A. E. Leanhardt, A. Görlitz, A. P. Chikkatur, D. Kielpinski, Y. Shin, D. E. Pritchard, and W. Ketterle, Imprinting vortices in a Bose-Einstein condensate using topological phases, Phys. Rev. Lett. **89**, 190403 (2002).

[41] C. Raman, J. R. Abo-Shaeer, J. M. Vogels, K. Xu, and W. Ketterle, Vortex nucleation in a stirred Bose-Einstein condensate, Phys. Rev. Lett. **87**, 210402 (2001).

[42] K. W. Madison, F. Chevy, W. Wohlleben, and J. Dalibard, Vortex formation in a stirred Bose-Einstein condensate, Phys. Rev. Lett. **84**, 806 (2000).